Preprint typeset using LaTeX style emulateapj v. 08/22/09

UPDATED CORRELATION SPECTRA FOR ANALYSIS OF THE DGL

Blake Chellew

ABSTRACT

We measure the DGL by correlating light intensity at an array of wavelengths with 100 micron intensity, following the example of Brandt & Draine (2012). We make two modifications to improve the spectra: one is updating the model to take optical depth (τ) into account, and the other is using updated 100 micron values from the IRIS dataset. We first look at the effect of only changing the model, then of only switching to the IRIS data. We plot the entire correlation spectra as well as smaller ranges that include emission lines. We calculate the equivalent widths of these lines and use them to estimate the temperature of the ISM. The τ correction has a significant impact on the correlation spectrum, while the effect of the IRIS data seems indistinguishable from noise. Neither correction appears to affect the prediction of ISM temperature.

1. INTRODUCTION AND MOTIVATION

Our goal is to measure the spectrum of the Diffuse Galactic Light (DGL). From the spectrum of this light, we can extract information about stars and gas in the milky way. In addition, it is useful to know about this light because it contaminates all measurements of the sky.

The DGL is too dim to measure directly, so Brandt & Draine (2012), hereafter BD, correlated light intensity from blank sky spectra from Sloan Digital Sky Survey (SDSS; York et al. (2000)) with 100 micron radiation measured by the IRAS satellite. The blank sky spectra are taken at various sky locations, and with 4000 wavelengths at each location. The 100 micron radiation should serve as a map of intergalactic dust, so the correlation spectrum should tell us about the spectrum of light scattered by dust. As in BD, we calculate the maximum likelihood estimator for the proportionality constant α_λ as a function of wavelength. To do this we use the same technique as BD with two modifications.

First, BD uses a model that assumes light interacts with dust particles at most one time. This assumption breaks down when the dust has a high optical depth. BD got around that by masking sky fibers with high intensity values, but here we use an updated model that accounts for optical depth. We continue to mask the same values for the sake of comparison, but later we could begin to unmask those values. Schlafly & Finkbeiner (2011) provided a way to calculate extinction values as a function of wavelength from E(B-V) values. Using this we calculate optical depth at the location of each sky fiber as a function of wavelength.

Second, the 100 micron data used by BD comes from the IRAS satellite, and it it was processed by Schlegel et al. (1998), hereafter SFD. More recently there has been improved analysis on the IRAS data (Miville-Deschênes & Lagache 2006). This is known as the IRIS dataset, and we use the updated values in our analysis.

2. OBSERVATIONS AND METHODOLOGY

2.1. *Optical Depth Correction*

The model used by BD was:

$$\lambda I_{\lambda,sky,j,p} = \alpha_\lambda[(\nu I_\nu)_{100\mu\mathrm{m},j,p} - \langle(\nu I_\nu)_{100\mu\mathrm{m}}\rangle_p]$$

For our new model, we correct for optical depth by replacing I_ν with $I_\nu\left(\frac{1-e^{-\tau}}{\tau}\right)$ to get

$$y_{\lambda,j,p} = \alpha_\lambda x_{\lambda,j,p}$$

where $x_{\lambda,j,p}$ is given by

$$((\nu I_\nu)_{100\mu m}\left(\frac{1-e^{-\tau}}{\tau}\right)_\lambda)_{j,p} - \langle(\nu I_\nu)_{100\mu m}\left(\frac{1-e^{-\tau}}{\tau}\right)_\lambda\rangle_p$$

and

$$y_{\lambda,j,p} = \lambda I_{\lambda,sky,j,p}$$

Notice that x was previously a 1D array, but it is now a 2D array because τ is a function of wavelength.

We recalculated the correlation spectrum using this model; see the top panel of Fig. 1 to see it plotted along with the original spectrum, with a bin width of 50 Å. We did not mask the emission lines, although we could have if we wanted to show just the part of the spectrum that is due to starlight. We expect the emission lines to be due to emissions from gas.

To see some of the emission lines up close we also plotted in Fig. 2, without binning, the spectra from 4830 to 5040 Å and 6530 to 6770 Å.

2.2. *Using IRIS Data*

We went through the same steps to calculate the correlation spectrum again, this time using the original model and the IRIS data. We wanted to see how the IRIS data would affect the result independent of changing the model. See the middle panel of Fig. 1, as well as Fig. 4, for plots of the spectrum.

Before performing the analysis, we compared the SFD 100 micron intensity values to the IRIS values at the same locations; see Fig. 3. The IRIS values are generally larger; in fact, they appear to be larger by a constant, in addition to some scatter. This would not affect the correlation if we used a general linear model. As it is, we use a linear model that passes through the origin, so there will be some effect on the correlation but if k is small it could be negligible. More interestingly, there appears to be a second cluster of points above the main linear cluster, but this is a minority of the points if we zoom out fully.

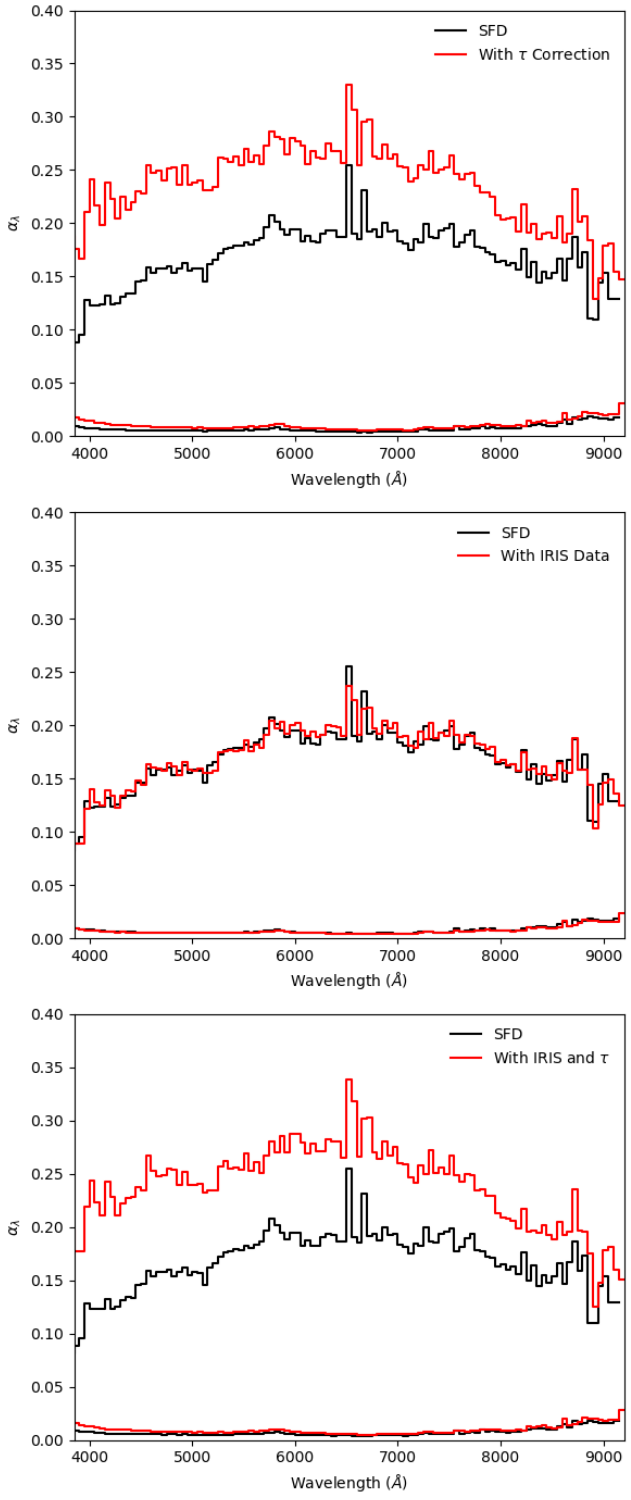

FIG. 1.— Correlation spectra calculated by correlating intensity from blank sky regions at various wavelengths with 100 micron intensity. The αs are binned with a bin width of 50 Å. The black spectrum in each panel, labeled "SFD," is our reproduction of the spectrum from Brandt & Draine (2012). The red spectra include modifications: the one in the top panel includes an updated model that accounts for optical thickness, the one in the middle panel uses IRIS data, and the one in the bottom panel uses both.

TABLE 1
H-α RATIOS

Line	SFD	τ Correction	IRIS	τ and IRIS
4960 (OIII)	0.12 ± 0.07	0.12 ± 0.07	0.11 ± 0.07	0.11 ± 0.08
5008 (OIII)	0.07 ± 0.07	0.06 ± 0.07	0.09 ± 0.08	0.09 ± 0.08
6550 (NII)	0.18 ± 0.04	0.19 ± 0.04	0.19 ± 0.04	0.20 ± 0.04
6585 (NII)	0.49 ± 0.05	0.50 ± 0.04	0.50 ± 0.05	0.52 ± 0.05
6718 (SII)	0.43 ± 0.05	0.43 ± 0.04	0.44 ± 0.05	0.43 ± 0.05
6733 (SII)	0.32 ± 0.04	0.33 ± 0.04	0.32 ± 0.04	0.33 ± 0.04

TABLE 2
H-β RATIOS

Line	SFD	τ Correction	IRIS	τ and IRIS
4960 (OIII)	0.31 ± 0.24	0.27 ± 0.20	0.28 ± 0.24	0.23 ± 0.20
5008 (OIII)	0.19 ± 0.23	0.14 ± 0.18	0.23 ± 0.23	0.19 ± 0.20
6550 (NII)	0.47 ± 0.19	0.42 ± 0.15	0.48 ± 0.19	0.43 ± 0.15
6585 (NII)	1.28 ± 0.35	1.13 ± 0.26	1.27 ± 0.35	1.13 ± 0.27
6718 (SII)	1.12 ± 0.32	0.95 ± 0.23	1.10 ± 0.31	0.93 ± 0.24
6733 (SII)	0.84 ± 0.26	0.73 ± 0.19	0.81 ± 0.26	0.70 ± 0.20

2.3. *Equivalent Width*

Looking at the emission lines in Figs. 2 and 4, we recognize them as Hβ 4863, [OIII] 4960, [OIII] 5008, [NII] 6550, Hα 6565, [NII] 6585, [SII] 6718, and [SII] 6733. We would like to measure the peaks quantitatively. A common way to do this is to calculate the equivalent width, which is a measure of the strength of the peak. It is defined as the width of a rectangle that contains the same amount of flux as the peak and has the same height as the continuum. The continuum is what the spectrum would look like in the absence of emission and absorption lines.

More formally, we apply the following formula:

$$W_\lambda = \int \left(\frac{F_\lambda - F_0}{F_0} \right) \mathrm{d}\lambda$$

where F_λ is the entire spectrum and F_0 is the continuum. Note that our data is discrete so we use a sum instead of an integral.

We estimated the continuum as follows. For the lines between 6500 and 6800 Å, we followed the example of BD and averaged the intensity of the spectrum between 6600 and 6700 Å. Based on the right panel of Fig. 2, this region does not appear to contain any emission lines. From Fig. 1 we can see that the continuum level is changing with wavelength, but it appears relatively flat between 6000 and 8000 Å. We also use the same wavelength ranges as BD for the Hβ lines. For the OIII lines, we averaged the values between 4900 and 4958 and between 4963 and 5000. These are regions to the left and right of the 4960 Å peak; we made sure not to include either of the OIII peaks in the range.

We integrated the spectrum near each of the peaks, including three wavelength elements on either side. After finding the equivalent widths, we calculated the ratio between each peak and the Hα and Hβ peaks. These results are shown in Tables 1 and 2. To estimate the uncertainty we found the standard deviation of the values that we used to calculate the continuum, then used the standard deviation as our uncertainty on each data point when calculating the equivalent width.

As in BD, we need to make corrections to the equiv-

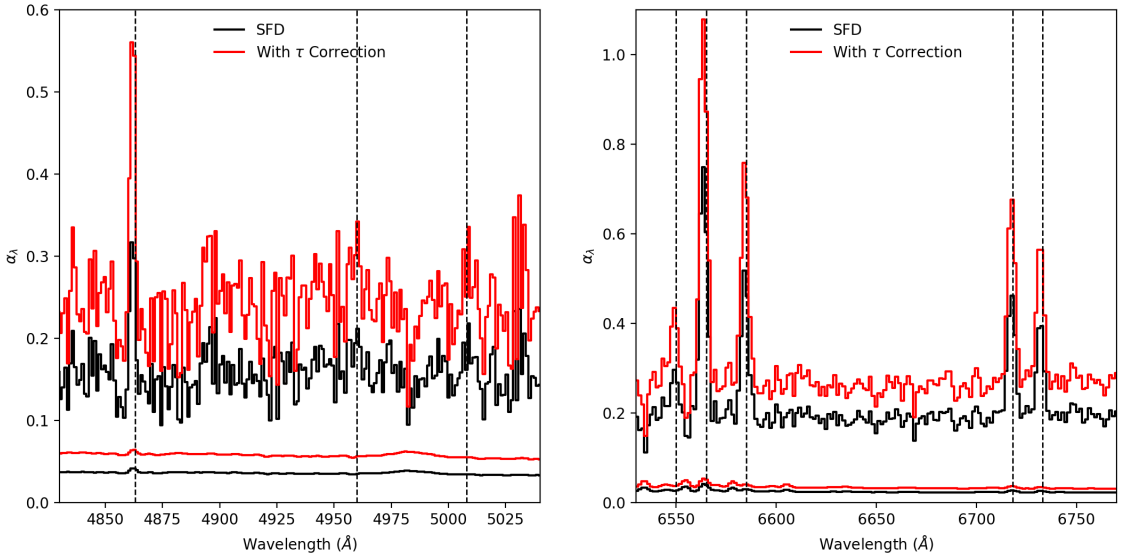

FIG. 2.— The correlation spectrum from the top panel of Fig. 1, but here it is not binned. This corrected spectrum uses a model that accounts for optical thickness of dust. It is larger than the original spectrum (in black) nearly everywhere, indicating better correlation.

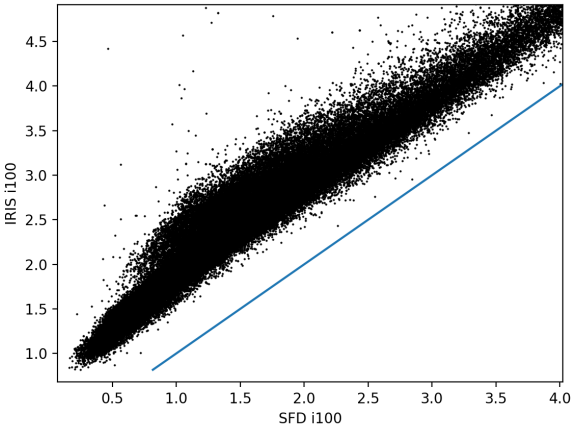

FIG. 3.— Scatterplot of the IRIS 100 micron values vs. SFD 100 micron values. The blue line is y = x; if the IRIS values were exactly the same as the previous values, all points would be on the line. It looks like there is a constant offset for most of the points, along with some scatter. There also appears to be a second cluster of points slightly more offset from the y = x line.

alent widths of Hα and Hβ because absorption lines for both of these are present in stars. Based on the size of the 4000 Å break, we calculate how much absorption we expect, then add that to the equivalent width we calculated.

3. DISCUSSION AND CONCLUSIONS

3.1. *Comparison to BD*

Before calculating any of the other correlation spectra, we first reproduced the spectrum from BD; our reproduction is the spectrum labeled "SFD" in Figs. 1, 2, 4, and 5. The shape of the reproduction appears nearly identical, but the values are slightly too high. This could be due to the fact that we used the actual wavelengths of the measurements and did not interpolate onto a more uniform wavelength array. We should still be able to compare the reproduced spectrum with our updated spectra because we used the same procedure for all of them. Note also that shifting the bins by 25 Å resulted in wider peaks near the center (around 2 bins wide instead of 1) and less obvious Mg absorption, although this effect is not present in Figs. 2 and 4 because there is no binning there. Given that we were able to closely reproduce the spectrum from BD, we can confirm that the source of the light appears to be scattered starlight based on the blueness of the spectrum, the 4000 Å break, and the absorption around 5170 Å. (There are several major Fraunhofer lines in the vicinity: Mg at 5184, 5173, and 5167 Å, and Fe at 5169 Å).

Our reproduced values for the ratios in Tables 1 and 2 were also not exactly as expected; we consistently found smaller values both for the equivalent widths and the ratios. This could be related to the values of α being too high, which results in a higher continuum and lower equivalent widths. Once again, in this paper we will mainly be concerned with relative values because we want to see how the results are affected by the modifications.

We also confirmed the statement from BD that the OIII lines are detected at low significance. For example, in the reproduced spectrum, we found the equivalent width of [OIII] 5008 as 0.77 ± 0.77 so that a 67% confidence interval includes 0.

3.2. *Spectrum with Optical Depth Correction*

Next we compare the original spectrum to the spectrum obtained using the model that incorporates optical depth. See Fig. 2. At first glance the new spectrum has generally the same shape. The main difference is that the updated spectrum has larger αs overall, ranging from nearly the same at redder wavelengths to much

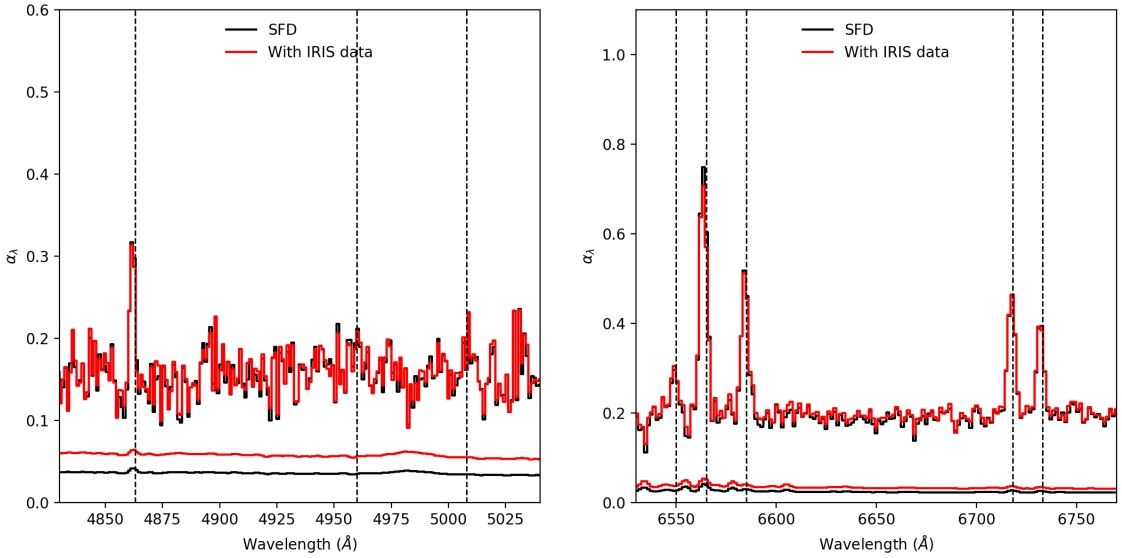

FIG. 4.— The correlation spectrum from the middle panel of Fig. 1, but here it is not binned. The corrected spectrum uses data from IRIS for the 100 micron intensity instead of data from the SFD maps. There is no systematic difference from the original spectrum; all the variation seems consistent with noise.

larger at bluer wavelengths. The updated spectrum is now clearly skewed towards the red, with larger values towards the blue, which makes sense because we expect blue light to scatter more. The previous model probably made it look like there was less blue light because of this; when blue light scatters on the way to our telescopes it will no longer reach us and we will not detect it.

There appear to be some important differences, but it turns out these are due to binning effects. The large emission peaks between 6000 and 7000 Å appear wider, but they are not, which we know because the peaks are the same width in Fig. 2 where the data is not binned. The Mg absorption seems wider and the 4000 Å break seems larger, but in fact if we shift the bins by 25 Å these issues disappear. The reason we do not display all plots with this shift is that it distorts the peaks and breaks in the original spectrum. Clearly we will have to work with the unbinned data for a good quantitative analysis.

In Fig. 2 we show the same comparison, but for selected wavelength ranges and unbinned. The result is consistent with what we see in the overall spectrum; the updated spectrum is higher almost everywhere. Both the continuum levels and peak heights appear different, so we need to look at the equivalent widths for an effective comparison. The line strengths from the updated model are all stronger, which means the emission lines are increasing more than the continuum. But we are more interested in the ratios of the lines to Hα and Hβ, which we will use for further analysis, and which are given in Tables 1 and 2.

As in BD, we calculate the ratio of [NII] 6585 to [NII] 6550 as a sanity check. We get 2.7 ± 0.7, which matches the predicted value of 3. We also perform this check for the other correlation spectra that we find, and the results look good.

3.3. *Spectrum with IRIS data*

Next we compare the spectrum calculated using IRIS data to the original spectrum. The full spectrum is shown in the middle panel of Fig. 1. It follows the original spectrum almost exactly; all the variation appears small enough to be consistent with noise. While the black peaks near the center appear to be taller than the red, if we shift the bins over by 25 Å the red peaks become taller. Similarly, we might worry that the Mg break does not appear in the updated spectrum, but if we shift the bins it shows up more prominently. Indeed, looking at the unbinned spectra in Fig. 4, we see that the spectra are much more similar than indicated by Fig 1. Looking at it quantitatively, the entries in Tables 1 and 2 confirm that there is virtually no difference between the emission lines: most of the differences are 0.01 or 0.02, just a fraction of the typical uncertainty. Evidently our prediction that the results would be insensitive to the offset that we saw in Fig. 3 was correct.

3.4. *Both Corrections Together*

We expect to be able to identify all the relevant changes to the spectrum by first changing only the model, to account for optical depth, then only switching to the IRIS data. After we did this, we performed the same analysis using both corrections together to make sure everything looked as expected. The continuum is shown in the bottom panel of Fig. 1 and the emission lines are shown in Fig 5. Each of Tables 1, 2, and 3 also include a column for this analysis.

There are no apparent surprises; the overall spectrum has the shape of the IRIS spectrum at the height of the τ spectrum, and Fig. 5 supports this conclusion. Finally, we see that the effects add when the corrections are in the same direction, as in the [NII] 6585 row of Table 1, and they cancel when in opposite directions, as in the [OIII] 5008 row of Table 2.

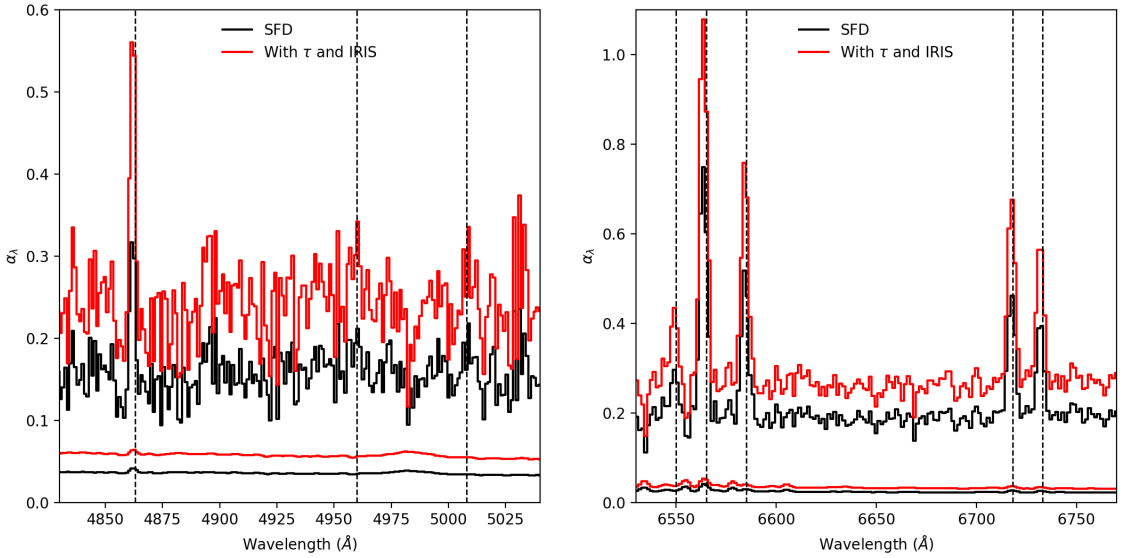

FIG. 5.— The correlation spectrum from the bottom panel of Fig. 1, but here it is not binned. This spectrum uses both the updated model and the IRIS data. It looks like we expect; it is shifted upwards due to the updated model, just like in Fig. 2, and it is just slightly different from that figure due to the use of the IRIS data.

TABLE 3
ISM TEMPERATURE RANGES

	SFD	τ Correction	IRIS	τ and IRIS
Lower Limit	7280	7280	7300	7300
Upper Limit	8250	8320	8320	8420

3.5. *Calculating ISM Temperature*

Finally, as in BD, we calculate ratios of [SII](6718 + 6733) and [NII](6550 + 6585) to Hα and use them to find estimates for the ISM (Interstellar Medium) temperature. We did not calculate curves to predict the ratio as a function of temperature; instead, we used the curves in Fig. 12 of BD. This gives us two temperature ranges, one for SII and one for NII, and we combine them to get the ranges in Table 3. This is consistent with Fig. 7 of Madsen et al. (2006). The temperatures do not appear to change much with the new models; the lower limit stayed virtually the same and the upper limit increased only slightly for both corrections.

REFERENCES

Brandt, T. D., & Draine, B. T. 2012, ApJ, 744, 129
Madsen, G. J., Reynolds, R. J., & Haffner, L. M. 2006, ApJ, 652, 401
Miville-Deschênes, M. A., & Lagache, G. 2006, in Astronomical Society of the Pacific Conference Series, Vol. 357, The Spitzer Space Telescope: New Views of the Cosmos, ed. L. Armus & W. T. Reach, 167
Schlafly, E. F., & Finkbeiner, D. P. 2011, ApJ, 737, 103
Schlegel, D. J., Finkbeiner, D. P., & Davis, M. 1998, ApJ, 500, 525
York, D. G., Adelman, J., Anderson, J., John E., et al. 2000, AJ, 120, 1579